ChemComm

FEATURE ARTICLE

View Article Online
View Journal | View Issue

Cite this: *Chem. Commun.*, 2025, **61**, 13601

Single-atom catalysts toward electrocatalytic urea synthesis *via* C–N coupling reactions

Zhiwei Wang,[a] Mingying Chen,[b] Guolong Lu,[b] Jianben Xu,*[c] Longchao Zhuo,[d] Yinghong Wu*[e] and Xijun Liu *[a]

Urea, with a global annual production that exceeds 200 million tons, occupies an irreplaceable position in agriculture, pharmaceuticals, and materials science. The conventional Haber–Bosch process and its derivatives are constrained by high energy consumption and considerable carbon emissions. Global urea production, for instance, utilizes approximately 1.4–2% of total energy, accompanied by 1.5–2.0 tons of CO_2 emissions per ton of product. Electrocatalytic technology utilizes a simultaneous reduction of CO_2 and nitrogen-containing compounds to achieve urea synthesis, offering advantages such as ambient temperature and pressure operation, renewable energy driving, and the potential for carbon neutrality. Life cycle assessments have indicated the potential for a 75% reduction in carbon footprint. Single-atom catalysts (SACs), distinguished by their atomically dispersed active sites, the ability to precisely adjust their coordination environments, and an extremely high metal atom utilization, have demonstrated remarkable efficacy in electrocatalytic urea synthesis. Following the initial report of Co–N–C SAC catalyzed urea synthesis in 2020, the field has witnessed a rapid expansion in related research, with a notable increase in urea faradaic efficiency (FE) from approximately 2% to 60.11% and substantial improvements in production rates, reaching 212.8 ± 10.6 mmol h^{-1} g^{-1}. This review systematically summarizes the advancements in SACs based on carbon-based, two-dimensional materials, metal–organic frameworks, and metal oxide supports. It delves into the regulatory mechanisms of supports on the electronic structure and coordination environment of active centers, while emphasizing the C–N bond formation mechanisms under diverse nitrogen sources. It also discusses the main challenges and future development directions in this field, providing theoretical and experimental guidance for the design of efficient electrocatalytic urea synthesis catalysts.

Received 9th June 2025,
Accepted 7th August 2025

DOI: 10.1039/d5cc03239c

rsc.li/chemcomm

1 Introduction

Urea, with a chemical formula of $(NH_2)_2CO$, is a vital compound with a global production that exceeds 200 million tons. It plays an indispensable role in agriculture, medicine, the chemical industry, and materials science, accounting for over 60% of global nitrogen fertilizer consumption and directly impacting global food security.[1–3] In the context of a rapidly expanding global population, the importance of urea, an essential nitrogen fertilizer, cannot be overstated. However, the traditional Haber–Bosch-based urea synthesis method is characterized by substantial drawbacks. The elevated temperature and pressure conditions necessitated by this method result in substantial energy consumption, accounting for 1.4–2% of global energy use, with the production of 1.5–2.0 tons of CO_2 emissions for each ton of urea produced.[4–6] Moreover, the reliance on robust raw materials, the prevalence of equipment corrosion, and constraints in large-scale production impede its sustainable development. In response to these issues, electrocatalytic urea synthesis has emerged as a promising alternative technology. This approach directly synthesizes urea by simultaneously reducing CO_2 and nitrogen-containing compounds at ambient temperature and pressure. It reduces energy consumption by 40–60%, enables carbon-neutral processes driven by renewable electricity, and integrates CO_2 emission reduction with resource utilization. Its modular nature lends itself to decentralized production, and life cycle

[a] *MOE Key Laboratory of New Processing Technology for Nonferrous Metals and Materials, Guangxi Key Laboratory of Processing for Non-ferrous Metals and Featured Materials, School of Resources, Environment and Materials, Guangxi University, Nanning, Guangxi, 530004, China. E-mail: xjliu@gxu.edu.cn*
[b] *School of Chemistry and Chemical Engineering, Guangxi University, Nanning, 530004, China*
[c] *Chongzuo Key Laboratory of Comprehensive Utilization Technology of Manganese Resources, Guangxi Key Laboratory for High-value Utilization of Manganese Resources, Guangxi Minzu Normal University, Chongzuo, Guangxi, 532200, China. E-mail: xujianben@163.com*
[d] *School of Materials Science and Engineering, Xi'an University of Technology, Xi'an, 710048, China*
[e] *National Engineering Research Center of Green Recycling for Strategic Metal Resources, Institute of Process Engineering, Chinese Academy of Sciences, Beijing, 100190, China. E-mail: yhwu@ipe.ac.cn*

assessments indicate the potential for a 75% reduction in carbon footprint.[7–10] Despite these advantages, electrocatalytic urea synthesis faces significant scientific challenges, including the efficient simultaneous activation of CO_2 and nitrogen sources to form C–N bonds, the thermodynamic stability of CO_2, the triple bond structure of N_2, precise control of NO_3^- reduction and NH_3 oxidation intermediates, and synergistic multi-step reactions at the same catalytic interface while suppressing competing reactions. These factors underscore the pivotal role of catalyst design in facilitating breakthroughs in electrocatalytic urea synthesis technology.[11–15]

Single-atom catalysts (SACs) are frontier catalytic materials that have emerged over the past decade. These catalysts are characterized by atomically dispersed metal active centers anchored precisely on specific supports. In comparison to traditional nanoparticle catalysts, SACs exhibit markedly different properties.[16–19] From a structural standpoint, SACs integrate the uniform active sites of homogeneous catalysts with high stability and facile separation of heterogeneous catalysts, thereby conferring a set of distinctive advantages. Firstly, isolated single-atom active sites maximize metal atom utilization, improving atomic efficiency by 10–100 times in comparison with conventional nanoparticle catalysts. Secondly, the strong interactions between single atoms and supports create special coordination environments, enabling fine-tuning of electronic structures. Thirdly, single-dispersed active centers avoid surface energy heterogeneity, enhancing reaction selectivity. Finally, uniform active sites simplify structure–activity relationship analysis, providing a foundation for rational design. The utilization of high metal dispersion or SACs is regarded as the optimal approach for the fabrication of heterogeneous catalysts that exhibit maximal activity at the atomic level for target reactions.[20–25] Since Wang *et al.* first reported the use of a Co–N–C SAC as a catalyst for the electrocatalytic synthesis of urea from CO_2 and NO_3^- in 2020, research in this field has undergone explosive growth. In a span of merely four years, the number of research articles pertaining to this subject has surpassed 200. SACs featuring various metal centers (*e.g.*, Cu, Fe, Co, Ni, Mn, and Mo) and diverse support materials (*e.g.*, carbon-based, oxides, MOF derivatives, and MXenes) have been developed successively. Remarkable advances have been made in catalytic performance, with FE of urea demonstrating a substantial enhancement, rising from approximately 20% initially to the highest reported value of 60.11%. Furthermore, there has been a notable increase in production rates, which have escalated from a few mmol h^{-1} g^{-1} to over 212.8 ± 10.6 mmol h^{-1} g^{-1}. These studies have not only expanded the application prospects of SACs in electrocatalysis but also deepened the understanding of C–N bond formation mechanisms. Notwithstanding the substantial progress that has been made, electrocatalytic urea synthesis continues to confront challenges, including inadequate activity, deficient selectivity, suboptimal stability, and ambiguous mechanisms.

This review aims to provide a systematic summary of the research progress pertaining to SACs for electrocatalytic urea synthesis. The categorization of catalysts is based on support types, which include carbon-based, two-dimensional materials, metal–organic frameworks, and metal oxides. A comprehensive analysis is conducted to elucidate the role of support materials in regulating the electronic structure, the coordination environment, and the catalytic performance of active centers. The article also discusses the main challenges and future development directions in the field, providing theoretical guidance and experimental references for designing efficient catalysts for electrocatalytic urea synthesis, thereby accelerating the transition of this technology from fundamental research to practical applications.

2 Mechanistic analysis of urea synthesis involving different nitrogen sources

Electrosynthesis of urea (ESU) is a complex reaction process involving multiple key steps, including co-activation, NO_x reduction, CO_2 reduction, and C–N coupling reactions.[26] It is imperative to acknowledge that these critical reaction steps do not occur independently; rather, they interact and depend on each other. Collectively, they participate in the ESU process. To achieve efficient and highly selective urea synthesis, precise control over the conditions and catalyst properties for each key reaction step is required to enhance catalytic efficiency and product selectivity. Concurrently, a comprehensive understanding of these fundamental reaction steps enables the optimization of the ESU system, thereby enhancing reaction efficiency. In the following sections, we will meticulously delineate the mechanistic pathways of disparate nitrogen sources implicated in urea synthesis. The electrochemical production of urea entails intricate chemical reactions, wherein nitrogen from diverse sources and CO_2 are transformed into urea under certain conditions, as described below:

Using NO_3^- as a nitrogen source for urea synthesis:

$$2NO_3^- + CO_2 + 18H^+ + 16e^- \rightarrow NH_2CONH_2 + 7H_2O$$

Using NO_2^- as a nitrogen source for urea synthesis:

$$2NO_2^- + CO_2 + 14H^+ + 12e^- \rightarrow NH_2CONH_2 + 5H_2O$$

Using NO as a nitrogen source for urea synthesis:

$$2NO + CO_2 + 10H^+ + 10e^- \rightarrow NH_2CONH_2 + 3H_2O$$

Using N_2 as a nitrogen source for urea synthesis:

$$N_2 + CO_2 + 6H^+ + 6e^- \rightarrow NH_2CONH_2 + H_2O$$

Furthermore, the spatial proximity of reactants and intermediates during the C–N coupling process is imperative for the efficient formation of urea. To facilitate comprehension of these intricate internal relationships, Fig. 1 illustrates the formation pathways of different C–N bond intermediates. A thorough examination of the intermediates and reaction pathways involved in urea synthesis can offer valuable theoretical insights for the design of high-performance catalysts.

The successful execution of the C–N coupling reaction in electrocatalytic urea synthesis is contingent upon the precise

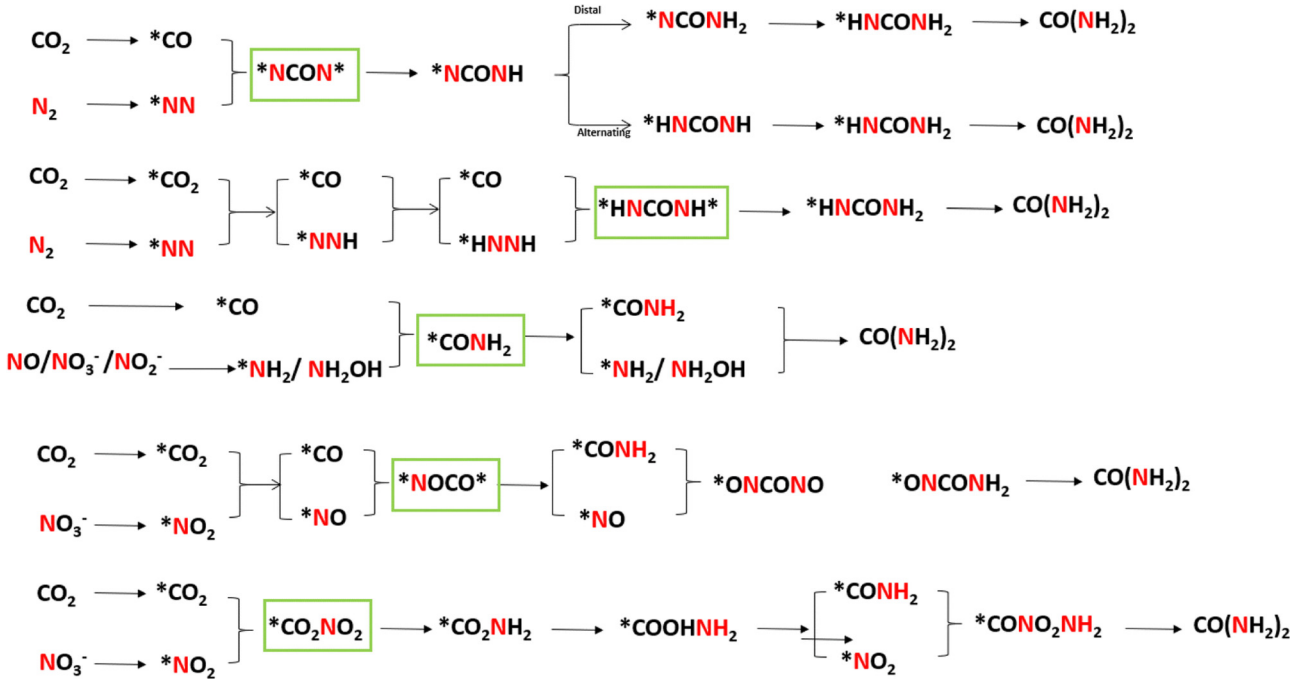

Fig. 1 Reaction pathways for the synthesis of urea by C–N coupling and its intermediates. Reproduced with permission from ref. 27. Copyright 2024, Green Chemistry.

formation, activation, and effective coupling of carbon-containing and nitrogen-containing intermediates. The carbon-containing intermediates principally comprise CO, the most critical carbon source with moderate binding strength and high reactivity, and COOH, the initial product of CO_2 reduction that can be further converted into more reactive CO. Nitrogen-containing intermediates principally consist of NH_2, the most critical nitrogen intermediate with suitable reactivity and stability. It is capable of forming C–N bonds with CO. The stability of these intermediates and their conversion kinetics directly determine the overall efficiency and selectivity of the reaction. Achieving efficient C–N coupling is contingent upon synergistic stabilization of CO and N_2 intermediates. The electronic structure of CO is more favorable for orbital hybridization with nitrogen intermediates, which results in a lower C–N coupling energy barrier for CO compared to COOH. Three main C–N coupling mechanisms have been identified, including the sequential coupling mechanism where pre-formed CO and NH_2 intermediates directly couple to form urea molecules, the synergistic coupling mechanism involving the activation and direct coupling of CO_2 and nitrogen sources, and the radical coupling mechanism where coupling reactions occur through radical intermediates under specific electrochemical conditions. However, selectivity remains the primary challenge in electrocatalytic urea synthesis, as it competes with reactions such as hydrogen evolution, CO_2 reduction to other products, and NO_x reduction leading to NH_3 formation.

2.1 HNO_3

The solubility of nitrate is significantly higher than that of inert nitrogen gas, which suggests that NO_3^- species can participate more effectively in aqueous-phase reactions. Additionally, the dissociation energy of the N=O bond in nitrite is relatively low, rendering nitrate/nitrite chemically more reactive and more likely to react with other substances.[28,29] As indicated by the high solubility of nitrate and the low dissociation energy of the N=O bond, nitrate (NO_3^-) couples with CO_2 to form urea more readily than inert N_2 molecules.

To elucidate the reaction mechanism, Mao *et al.*[30] unveiled two potential pathways for the C–N coupling reaction over graphene–In_2O_3 catalysts. One pathway involves the reduction of NO_3^- to NO_2^-, followed by further reduction to generate the key intermediate NH_2, which directly combines with CO_2 to produce urea. The remaining portion combines with H to form NH_3. The other pathway is that NO_2, generated from NO_3^- reduction, directly couples with CO_2 to form urea. These findings are of great significance for understanding the reaction mechanism (Fig. 2a).

Recently, Chen *et al.*[31] reported a $CuPd_1Rh_1$–DAA diatomic alloy catalyst, revealing that its synergistic tandem catalytic mechanism involving Pd_1–Cu and Rh_1–Cu active sites effectively promotes the electrosynthesis of urea. Specifically, the Pd_1–Cu site primarily catalyzes the early-stage C–N bond formation, facilitating the conversion of the intermediate CO_2NO_2 into CO_2NH_2; meanwhile, the Rh_1–Cu site accelerates the protonation of CO_2NH_2 to $COOHNH_2$. The cooperative effect of these two sites significantly enhances the urea yield (Fig. 2b). This study not only deepens the understanding of the reaction mechanism for NO_3^- electroreduction to urea but also provides new theoretical guidance and practical approaches for designing multi-active-site catalysts.

The process of synthesizing urea using nitrate as a nitrogen source consists of multiple stages, including nitrate reduction,

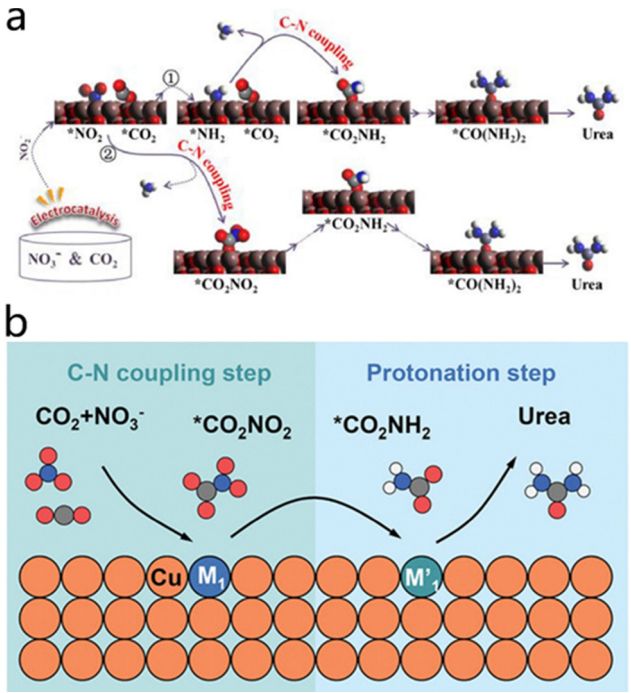

Fig. 2 (a) Two possible pathways for urea synthesis involving CO_2 and NO_3^-. Reproduced with permission from ref. 30. Copyright 2024, Chinese Chemical Letters. (b) Schematic of the tandem catalytic mechanism on Cu DAA. Reproduced with permission from ref. 31. Copyright 2024, Advanced Materials.

the nitrogen reaction with CO_2, the conversion of ammonium carbamate, the regulation of side reactions, and the selection of catalysts and electrolytes. Through the optimization of reaction conditions, the production of urea can be rendered both efficient and environmentally friendly. Despite the abundance of nitrate and the direct reduction process's capacity to yield nitrogen and water as feedstock for urea synthesis, this process necessitates substantial energy input and may be accompanied by undesirable side reactions, which can compromise the efficiency and selectivity of urea synthesis.

2.2 HNO_2

Nitrite (NO_2^-) functions as a nitrogen source and exhibits a unique reaction mechanism in the electrocatalytic reduction synthesis of urea. On the surface of the catalyst, nitrite accepts electrons and protons, undergoing a stepwise reduction process that generates nitrogen-containing intermediates, such as $*NH_2$ or *NH active species. These reduced nitrogen intermediates subsequently couple with activated CO_2 intermediates, resulting in the formation of essential nitrogen-containing carbon-based intermediates. Feng *et al.*[32] reported that the synergistic effect between Te and Pd in Te–Pd nanoclusters significantly promotes the CO_2 reduction reaction to produce CO and the nitrite reduction reaction to generate NH_2. Subsequently, these species undergo C–N bond coupling, ultimately enabling urea synthesis (Fig. 3a).

Zhao *et al.*[33] designed a Ru–Cu_3N catalyst system that provides a typical demonstration of this mechanism. This catalyst achieves

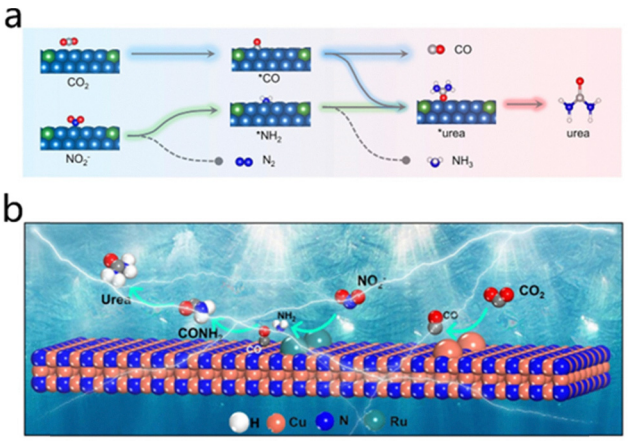

Fig. 3 (a) Urea synthesis from CO_2RR and NO_2RR on Te–Pd NCs. Reproduced with permission from ref. 32. Copyright 2020, Nano Letters. (b) Schematic of the ECNU process on Ru_1@Cu_3N. Reproduced with permission from ref. 33. Copyright 2024, Chemical Engineering Journal.

efficient activation and conversion of nitrite and CO_2 through the synergistic action of Ru and Cu active sites. As demonstrated in Fig. 3b, the Cu sites exhibit a preference for catalyzing the reduction of CO_2 to produce the key intermediate CO, while the Ru sites are responsible for the reduction of nitrite to form the active nitrogen intermediate $*NH_2$. Subsequently, CO and $*NH_2$ undergo C–N coupling at the Ru sites to form nitrogen-containing carbon-based intermediates. These intermediates, in turn, undergo further proton and electron transfer steps, ultimately resulting in the formation of urea. The entire reaction process also involves a complex transfer of 14 protons and 12 electrons, fully reflecting the central role of HNO_2 as a nitrogen source. However, the utilization of nitrite is subject to certain limitations and must be strictly controlled, primarily due to its potential safety risks and environmental regulatory constraints.

2.3 NO

The mechanism of electrocatalytic urea synthesis *via* nitric oxide (NO) reduction consists of the following steps: during the electrocatalytic process, NO is initially activated and reduced, forming nitrogen-containing intermediates, which subsequently undergo C–N coupling with carbon-based intermediates from the CO_2 reduction reaction (CO_2RR). The outcome of this process is the production of urea. As summarized by Long *et al.*[34] concerning the NORR (NO reduction reaction) mechanism, the detection of ammonia (NH_3) in experiments indicates the presence of multiple possible nitrogenous intermediates such as NO*, HNO*, HNOH*, H_2NO*, H_2NOH*, NOH*, N*, NH*, and NH_2*.[35] Based on these intermediates, the initial C–N bond formation is consistent with 18 possible coupling reactions (Fig. 4a). Furthermore, Wan *et al.*[36] revealed that NO and CO can synergistically interact on copper catalysts to generate urea, highlighting that NO, due to its lower reduction energy barrier, dominates the competitive reaction with CO. The urea synthesis pathway involves two critical C–N coupling steps, with the formation of the initial C–N bond designated as the rate-determining step. These theoretical findings are consistent

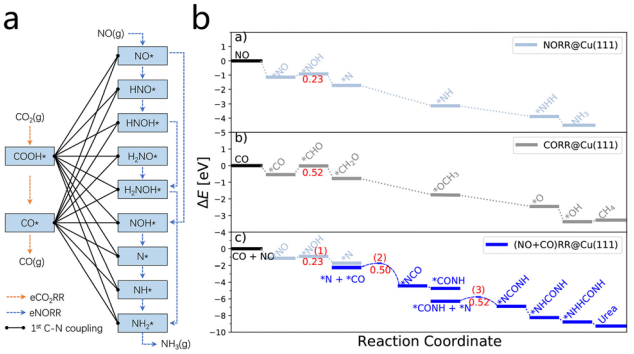

Fig. 4 (a) Schematic illustration of eCO_2RR, eNORR, and the first C–N coupling reactions. Reproduced with permission from ref. 34. Copyright 2024, ACS Catalysis. (b) Three reaction pathways on the Cu(111) surface energy diagram. Reproduced with permission from ref. 36. Copyright 2023, ACS Catalysis.

with experimental results, demonstrating an efficient electrocatalytic C–N coupling mechanism on copper-based catalysts. This finding suggests that the mechanism may be applicable to the synthesis of urea and other amide compounds (Fig. 4b).

It is noteworthy that NO, as a nitrogen source, exhibits higher energy efficiency in electrocatalytic reduction primarily because it can be reduced at lower potentials and its reduction products can directly participate in urea synthesis. However, the relatively limited availability of NO, and the significantly greater difficulty in obtaining it compared to molecular nitrogen (N_2), largely constrains its practical potential for industrial-scale urea synthesis.

2.4 N_2

The urea synthesis process consists of three primary stages: co-activation, C–N coupling reaction, and hydrogenation steps of reaction intermediates. In the presence of water, the reduction of N_2 and CO_2 to form urea is a six-electron transfer process, described by the following reaction: $N_2 + CO_2 + 6H^+ + 6e^- \rightarrow CO(NH_2)_2 + H_2O$. Among these, co-activation is a prerequisite for achieving urea synthesis.[37] Cao *et al.*[38] proposed several key reaction intermediates, such as HNCONH, $NCONH_2$, HNNH, and NNH_2, to evaluate the catalyst's ability to facilitate the electrochemical coupling of CO_2 and N_2 for urea synthesis. The detailed mechanism is illustrated in Fig. 5a. Initially, CO_2 undergoes a three-proton, three-electron transfer, which results in the generation of CO. Subsequently, CO couples with adsorbed N_2 *via* a C–N coupling reaction to form intermediates NCONH and *COOH. Subsequently, NCONH undergoes a four-electron transfer, which leads to two possible urea synthesis pathways. Cleavage of the N–N bond in COOH (also through a reduction process) opens two additional synthesis routes. Furthermore, Kong *et al.*[39] employed a Co/p-BN catalyst to facilitate the electrochemical coupling of CO_2 and N_2. Their study indicates that the urea synthesis pathway involves the reduction of CO_2 to CO, the coupling of CO with N_2 to form NCON, and a sequential four-step hydrogenation process that converts NCON into urea. As demonstrated in Fig. 5b, the rate-determining step

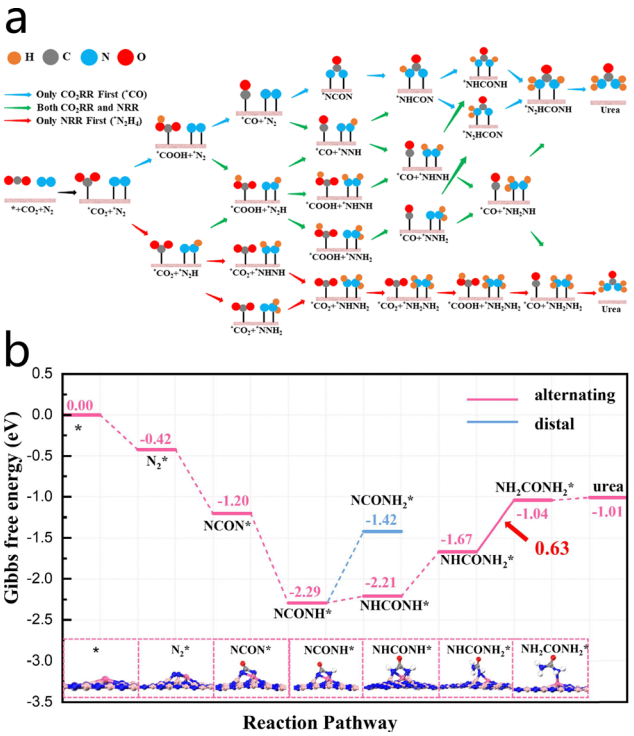

Fig. 5 (a) Mechanism diagram of the electrochemical coupling of CO_2 and N_2 to produce urea. Reproduced with permission from ref. 37. Copyright 2023, Journal of Materials Chemistry A. (b) Reaction energy barriers and the corresponding intermediate structures for urea electrosynthesis on the Fe/p-BN catalyst. Reproduced with permission from ref. 39. Copyright 2023, Chemical Engineering Journal.

is the hydrogenation of $NHCONH_2$, with an energy barrier of 0.63 eV, indicating a relatively low reaction energy barrier.

Molecular nitrogen is the most abundant nitrogen source in nature, and it offers high sustainability and theoretical atom economy because it does not rely on any chemical derivatives. However, the extremely stable N≡N triple bond in N_2 molecules requires highly active catalysts and substantial energy input for activation, which significantly limits its efficiency in various catalytic processes.

3 Catalyst types

Conventional nanoparticle catalysts exhibit constrained performance enhancement potential, attributable to the heterogeneity of active sites and the complexity in the suppression of side reactions. In contrast, SACs with their atomically dispersed structure provide isolated active site effects that significantly reduce side reactions while enhancing atomic utilization and selectivity. In the field of ESU, SAC systems predominantly comprise transition metal single atoms that are anchored onto functional supports, such as nitrogen-doped carbon materials, metal oxides, and graphitic carbon nitride. The fundamental attribute of SACs is rooted in the robust interaction between the metal atoms and the support, which functions to stabilize the single-atom structure. This interaction also facilitates precise modulation of the electronic structure and catalytic activity of

the metal atoms. The local coordination environment, such as the M–N_4 structure in nitrogen-doped carbon materials or the M–O structure in metal oxides, exerts a substantial influence on the adsorption configurations of reactant molecules and the catalytic performance, thereby determining the efficiency and selectivity of urea synthesis.

For instance, W–MoS_2 and Co–TiO_2 single-atom catalysts have demonstrated remarkable performance, with faradaic efficiency levels reaching up to 60.11% and urea yield as high as 212.8 mmol g^{-1} h^{-1}. These findings substantiate the revolutionary advantages of SACs in enhancing selectivity and activity. By optimizing the type of metal, coordination environment, and support properties, SACs open new possibilities for the development of electrocatalytic urea synthesis technologies.

3.1 Carbon-based supports

Carbon-based supports demonstrate extensive application prospects in electrocatalytic urea synthesis (ESU) due to their excellent physicochemical properties. Their high specific surface area and unique π-conjugated electronic structures provide abundant and uniform active sites for reactant adsorption and activation, significantly promoting reaction kinetics.[40,41] By meticulously adjusting catalyst morphology, surface oxygen-containing functional groups, and microstructural parameters, the adsorption configurations and reaction pathways of reactants on the catalyst surface can be efficiently regulated to achieve high selectivity in urea synthesis.[36] Moreover, carbon materials demonstrate outstanding structural stability and chemical tolerance, ensuring sustained stable catalytic performance under the severe conditions of electrocatalytic urea synthesis, a property that is of paramount importance for industrial applications. The present research endeavors are centered on the development of innovative carbon-based materials systems such as carbon-based SACs that exhibit precise metal–nitrogen coordination structures (*e.g.*, M–N–C) and graphitic carbon nitride (g-C_3N_4).[42] Both theoretical calculations and experimental studies have demonstrated that these catalysts not only maximize metal atom utilization but also significantly enhance catalytic activity and selectivity by modulating local electronic structures.

Theoretical calculations provide a foundational framework for the rational design of electrocatalysts. Systematic density functional theory (DFT) studies show that transition metal single atoms anchored on graphitic carbon nitride (TM@g-C_3N_4) exhibit considerable potential in electrocatalytic urea synthesis. Cheng *et al.*[43] conducted high-throughput computational screening and systematically evaluated 19 TM@g-C_3N_4 catalyst systems. It was determined that Ti@g-C_3N_4 exhibited not only remarkable catalytic activity but also commendable thermodynamic stability. To assess the influence of competing reactions, adsorption free energies (ΔG_{ad}) of H_2, CO_2, and N_2 on all TM@g-C_3N_4 catalysts were calculated. As demonstrated in Fig. 6a, with the exception of Ag, Cd, Mo, Zr, and Nb@g-C_3N_4, the adsorption free energies of N_2 and CO_2 were lower than that of H on the remaining catalysts. This finding suggests that the thermodynamic feasibility of the nitrogen reduction reaction (NRR) and the CO_2 reduction reaction (CO_2RR) exceeds that of the hydrogen evolution

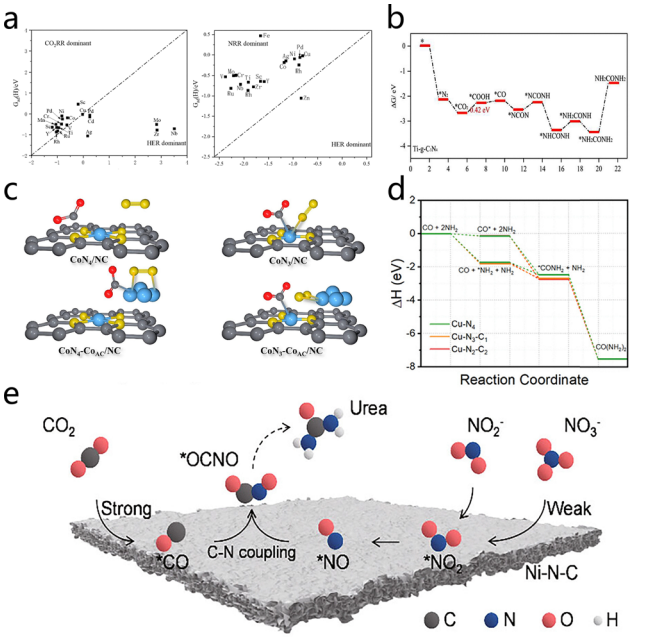

Fig. 6 (a) Adsorption Gibbs free energies of N_2, CO_2, and H on TM-*g*-C_3N_4. (b) Gibbs free energy diagram for urea synthesis *via* CO_2 and N_2 coupling. Reproduced with permission from ref. 43. Copyright 2023, Electrochimica Acta. (c) Simplified schematic of N_2 and CO_2 molecules on the catalysts surfaces. Reproduced with permission from ref. 44. Copyright 2025, Journal of Colloid and Interface Science. (d) Reaction pathway for urea production from simultaneous CO_2RR and NO_3RR. Reproduced with permission from ref. 45. Copyright 2022, Advanced Energy Materials. (e) Schematic diagram of the reaction pathway of electrocatalytic urea synthesis on Ni–N–C. Reproduced with permission from ref. 46. Copyright 2023, Carbon Energy.

reaction (HER) in the majority of catalyst surfaces. In the Ti@g-C_3N_4 system, $\Delta G_{ad}(N_2)$ and $\Delta G_{ad}(CO_2)$ were considerably lower than $\Delta G_{ad}(H)$, indicating a distinct benefit in the suppression of the HER. As illustrated in Fig. 6b, the free energy profile of CO_2 and N_2 activation and subsequent C–N coupling on Ti@g-C_3N_4 demonstrates a maximum energy barrier of only 0.41 eV, which is significantly lower than that of other transition metal catalysts. This study systematically elucidates the guiding role of theoretical calculations in electrocatalyst design, providing an important theoretical basis for developing efficient catalysts for electrocatalytic urea synthesis.

The experimental work of Zhao *et al.*[44] further validated the outstanding performance of SACs in ESU. The CoN_3–CoAC/NC catalyst, prepared *via* crystallization pyrolysis, exhibited a unique electronic delocalization effect, achieving a urea production rate of 20.83 mmol h^{-1} g^{-1} and a FE of 23.73% at −0.4 V *vs.* RHE. As illustrated in Fig. 6c, the relaxed atomic structures of chemically adsorbed inert reactants are observed on CoN_4/NC, CoN_4–CoAC/NC, CoN_3/NC, and CoN_3–CoAC/NC. The enhanced catalytic performance is attributed to the synergistic effect between cobalt clusters and single-atom sites, which results in a substantial reduction in reaction energy barriers. The study by Leverett *et al.*[45] revealed the critical influence of copper atomic coordination structures on reaction selectivity. The investigation revealed that both Cu–N_4 and Cu–N_{4-x}–C_x sites exhibited catalytically

active properties for the nitrate reduction (NO_3RR). However, it was observed that the Cu–N_4 sites demonstrated higher activity in reactions involving the reduction of CO_2. Furthermore, the study accomplished the first electrochemical synthesis of urea using Cu SACs by integrating CO_2RR and NO_3RR. As illustrated in Fig. 6d, the DFT-calculated urea synthesis pathway on Cu–N_4 sites demonstrates an enhanced catalytic activity as compared to the two counterparts. In experimental trials, a FE of 28% and a urea production rate of 4.3 nmol s^{-1} cm^{-2} were achieved, thereby establishing a novel utilization of SACs for the synergistic electrochemical urea synthesis *via* CO_2RR and NO_3RR. This series of studies not only deepened the understanding of SAC reaction mechanisms and selectivity but also highlighted the crucial role of combining theoretical calculations and experiments in catalyst design and performance optimization.

It is noteworthy that non-metal nitrogen-doped catalysts exhibit superior performance in ESU when compared to precious metal electrocatalysts. In a seminal study, Chen *et al.*[46] advanced an innovative catalyst design strategy by incorporating Ni single atoms into nitrogen-doped metal-free catalysts (N–C), thereby forming Ni–N-CSACs. When KNO_2 was utilized as a nitrogen source, the catalyst demonstrated a substantial enhancement in catalytic activity, with urea synthesis increasing by an order of magnitude compared to nitrate. This enhancement is attributable to the substitution of nitrogen sources and the optimization of reaction pathways, which collectively generate a substantial quantity of nitrogen-containing intermediates and rebalance the activity among side reactions (Fig. 6e). The developed nitrogen-doped carbon catalysts were able to achieve a urea production rate of 610.6 mg h^{-1} $g_{cat}{}^{-1}$, surpassing precious metal electrocatalysts. This breakthrough not only exemplifies the immense potential of N-doped carbon materials as metal-free catalysts in ESU but also provides novel insights into sustainable chemistry and green synthesis by effectively circumventing the utilization of rare or precious metals.

However, the industrial-scale application of carbon-based catalysts in the field of electrocatalytic urea synthesis (ESU) still faces numerous challenges, requiring further in-depth research and systematic validation. At present, researchers are committed to the development of innovative carbon-based catalytic systems that aspire to augment their intrinsic catalytic activity, long-term stability, and product selectivity. Concurrently, they are undertaking a comprehensive elucidation of the reaction mechanisms to facilitate the practical implementation and industrialization of ESU technology.

3.2 Two-dimensional materials

Two-dimensional (2D) materials have emerged as a prominent area of research interest within the broader context of electrocatalytic urea synthesis (ECU). This focus is largely attributed to the distinctive physicochemical properties exhibited by these materials, which include high specific surface areas, an abundance of active sites, and remarkable capability for electronic structure modulation. Theoretical calculations play a crucial role in catalyst design and screening, providing a solid foundation for elucidating catalytic mechanisms and guiding rational catalyst development. In the early stages of research, DFT was utilized to systematically screen catalysts. It was determined that transition metal single atoms anchored on graphitic carbon nitride (g-C_3N_4) supports exhibited promising catalytic activity. Among them, Ti@g-C_3N_4 catalysts stand out as typical representatives with a comparatively low energy barrier for urea synthesis (0.41 eV) and adequate thermal stability.[41] However, reliance on experimental screening and preliminary theoretical analysis alone is insufficient for achieving a comprehensive understanding of the intrinsic relationship between catalytic activity and the electronic structure. This limitation restricts the attainment of precise mechanistic insights and the development of precise catalyst design. To address this, researchers have developed more fundamental theoretical models. Xiong *et al.*[47] proposed a systematic screening strategy to investigate the catalytic performance of single-atom metals anchored on α-borophene nanosheets (M@α-B). Their study revealed that α-borophene catalysts anchored with metals such as Ti, Cr, Nb, Mo, and Ta exhibit excellent activity and selectivity for urea synthesis. The catalytic performance exhibits a close correlation with the d-band center position and charge density transfer of the active center atoms. Based on the constructed volcano plot relating limiting potentials to d-band centers (Fig. 7a), the researchers introduced a new descriptor, termed φ, to quantitatively interpret the correlation between atomic properties and catalytic performance. The results indicate that materials with limiting potentials between −0.4 V and 0 V and d-band centers within −0.2 to 0.8 eV exhibit augmented catalytic activity This observation provides a theoretical foundation for the screening of efficient urea synthesis catalysts. This work contributes to the theoretical understanding of the catalytic mechanism. However, the translation of theoretical predictions into practical catalytic systems still necessitates experimental validation.

Guided by theoretical frameworks, research has shifted towards 2D materials, characterized by specific structures and a high density of defects, with the objective of enhancing catalytic performance. Addressing the inadequate conductivity and insufficient exposure of active sites in g-C_3N_4, Kong *et al.*[39] developed a novel electrocatalyst by anchoring single metal atoms onto porous boron nitride (p-BN) nanosheets with dual vacancies. A high-throughput DFT screening revealed that Fe/p-BN and Co/p-BN catalysts not only exhibit excellent catalytic activity and selectivity but also show reduced kinetic barriers for the C–N coupling reaction. During the reaction, N_2 molecules preferentially adsorb in a side-on mode on catalysts such as Ti, V, Cr, Mn, Fe, Co, Ni, and Mo. In this configuration, the metal atom and its two adjacent boron atoms act as triple active sites, forming one metal–N and two B–N bonds (Fig. 7b and c), effectively promoting urea synthesis. This study, which integrates theoretical calculations and experimental verification, demonstrates the feasibility of tailoring SAC performance *via* support engineering. However, the intrinsically low conductivity of boron nitride-based materials may limit further enhancement of overall electrocatalytic performance.

To overcome the conductivity limitations, researchers have shifted their focus to highly conductive 2D material supports.

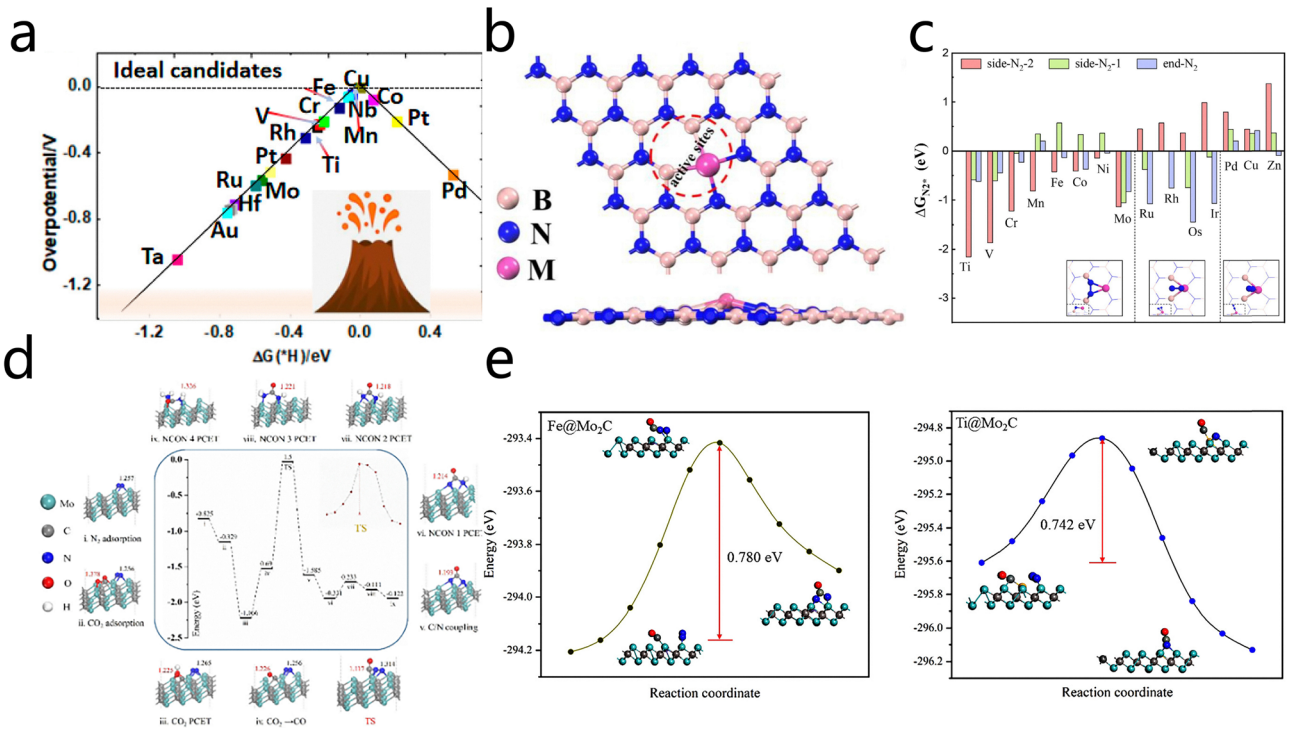

Fig. 7 (a) Volcano plots of calculated overpotentials toward the HER. Reproduced with permission from ref. 47. Copyright 2022, Chemistry of Materials. (b) Optimized structural model of catalyst M/p-BN. (c) Free adsorption energies of N2* (ΔGN_2*) *via* end/side-on patterns. Reproduced with permission from ref. 39. Copyright 2023, Chemical Engineering Journal. (d) Free energy change diagram of the minimum energy path of the CO_2/N_2 urea synthesis reaction, the atomic configurations of the reaction intermediates and the transition state energy change of *CO and *NN coupling reactions on the surface of Mo_2C. (e) Transition state energy variations for the C/N coupling reactions occurring on Fe@ Mo_2C and Ti@Mo_2C surfaces. Reproduced with permission from ref. 49. Copyright 2022, Chinese Journal of Structural Chemistry.

MXenes, a class of transition metal carbides/nitrides with graphene-like layered structures, possess a high surface area, abundant exposed active sites, and tunable electronic structures, showing broad potential in electrocatalysis.[48] Peng *et al.*[49] systematically studied the catalytic activity of Mo_2C–MXene catalysts for co-reduction of N_2 and CO_2 to synthesize urea *via* DFT. The results of the study indicate that although the bare Mo_2C surface favors urea synthesis, its relatively high transition state energy barrier (~1.50 eV) limits catalytic efficiency (Fig. 7d). The implementation of single-atom loading strategies, particularly those involving Fe and Ti single atoms, results in a substantial reduction in the energy barrier associated with the transition state for C–N coupling. This observation is exemplified by Ti@Mo_2C that exhibited superior catalytic selectivity and activity. This finding underscores the considerable promise of MXenes as the support for SACs (Fig. 7e). This study integrates theoretical calculations with experimental research, thereby advancing electrocatalytic urea synthesis. However, the prevailing focus of contemporary research is on the synergistic pathways of the CO_2 reduction reaction (CO_2RR) and the nitrogen reduction reaction (NRR), while alternative potential reaction pathways warrant further exploration.

Furthermore, two-dimensional transition metal sulfides, exemplified by MoS_2, have garnered interest for urea electrosynthesis due to their distinctive electronic structure and plentiful edge active sites. Du *et al.*[50,51] developed two efficient urea electrocatalysts: single-atom Cu anchored MoS_2 (Cu_1/MoS_2) and Fe single-atom loaded MoS_2 (Fe_1/MoS_2). The faradaic efficiencies of these catalysts were measured to be 54.98% and 57.02%, respectively, while the urea yields were found to be 18.98 and 23.3 mmol h^{-1} g^{-1}, respectively. In these catalysts, single metal atoms form isolated M_1–S_3 structures anchored on the MoS_2 surface. The M_1–S_3 active sites and MoS_2 edges synergistically promote C–N coupling and hydrogenation *via* a tandem mechanism: as illustrated in Fig. 8a, the former process is predominant in the initial stages of C–N bond formation and NO_2^- reduction to CO_2NH_2. In contrast, the latter process plays a pivotal role in the subsequent hydrogenation of CO_2NH_2 to urea. In a related study, Yuan *et al.*[52] employed W SACs (W_1/MoS_2) to achieve co-reduction of CO_2 and NO_2^- to urea, reaching a maximum FE of 60.11% and a urea production rate of 35.80 mmol h^{-1} g^{-1} in a flow cell. As NO_2RR and the HER represent two major competing reactions in ECNU,[53] the selectivity of ECNU was evaluated by analyzing the NO_2RR and HER behavior on W_1/MoS_2. As shown in Fig. 8b, for NO_2RR, the W_1–S_3 site exhibits a preference for coupling with CO_2 over hydrogenation to form HNO_2. This observation indicates that W_1/MoS_2 exhibits a greater propensity for NO_2 and CO_2 C–N coupling as opposed to *NO_2 hydrogenation to NH_3. As demonstrated in Fig. 8c, for the HER, the adsorption free energy of NO_2^- on W_1–S_3 is more negative than that of hydrogen, indicating that W_1–S_3 exhibits a stronger preference for adsorbing NO_2^- over hydrogen.

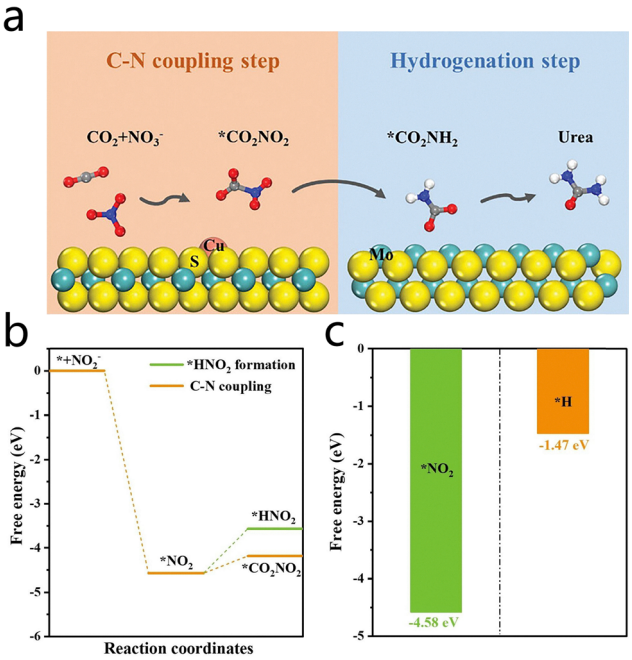

Fig. 8 (a) Schematic diagram of the tandem catalytic mechanism on Cu_1–MoS_2. Reproduced with permission from ref. 50. Copyright 2024, Advanced Energy Materials. (b) Free energy diagrams of C–N coupling and *HNO_2 formation on W1–S3. (c) Adsorption free energies for NO_2^- and H adsorption on W_1–S_3. Reproduced with permission from ref. 52. Copyright 2025, Journal of Colloid and Interface Science.

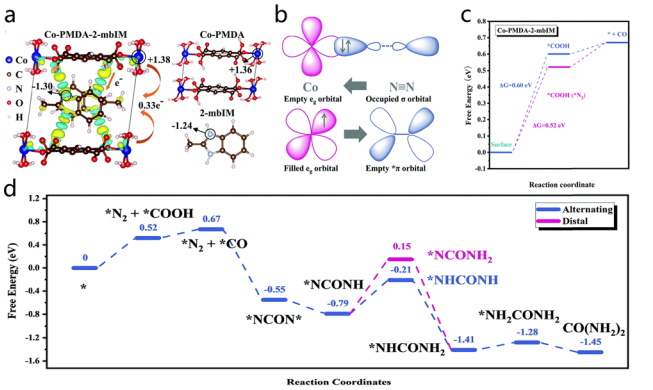

Fig. 9 (a) The charge density difference of Co-PMDA-2-mbIM and the corresponding results of Bader charge analysis. (b) A simplified schematic diagram of N_2 bonding to a Co center. (c) Free energy diagrams for CO_2 reduction with and without N_2 adsorption on Co-PMDA-2-mbIM. (d) The possible urea electrosynthesis mechanism. Reproduced with permission from ref. 55. Copyright 2022, Energy & Environmental Science.

These results suggest that the suppression of competing NO_2RR/HER on W_1–S_3 is effective, leading to high ECNU selectivity for urea production. This study provides novel insights into the design of W-based SACs and demonstrates the potential of electrocatalytic urea synthesis in the treatment of environmental pollutants and the production of high-value production urea.

2D material-based SACs exhibit remarkable catalytic activity and selectivity in the electrocatalytic synthesis of urea, a phenomenon that can be attributed to their excellent electronic structure modulation and the abundance of active sites present within the material. However, challenges persist regarding the conductivity, stability, and structural control of 2D materials. Consequently, there is a necessity to explore more highly tunable and multifunctional catalytic systems.

3.3 Metal–organic frameworks (MOFs)

In addition to metal oxides, metal–organic framework (MOF) catalysts have demonstrated tremendous application potential in the domain of electrocatalytic urea synthesis (ESU). MOFs are a class of porous materials composed of metal ions or clusters connected with organic ligands. The highly tunable structures and abundant surface-active sites of MOFs make them ideal candidates for ESU. It has been demonstrated that some MOFs inherently possess catalytic activity and can directly participate in the electrochemical synthesis of urea. For example, certain MOFs exhibit excellent electrocatalytic nitrogen fixation capabilities. Consequently, the employment of MOFs as catalysts not only streamlines the reaction system but also augments reaction efficiency.[54] At a potential of −0.5 V with respect to the reversible hydrogen electrode, the conductive Co–MOF composite catalyst developed by Yuan *et al.*[55] achieved a FE of 48.97% and a urea production rate of 14.47 mmol h^{-1} g^{-1}. This result establishes a new performance benchmark in the field. Fig. 9a elucidates the intrinsic mechanism underlying this catalytic performance through electron density difference analysis: the CoO_6 octahedron (cyan region) transfers approximately 0.33 electrons to the 2-mbIM organic ligand. Based on Bader charge analysis, the Co site in CoO_6 (charge +1.36) functions as a local electrophilic center, while the nitrogen atom in the 2-mbIM ligand (charge −1.24) acts as a nucleophilic site. Consequently, electron-rich N_2 molecules and electron-deficient CO_2 molecules tend to adsorb on the electrophilic Co sites of CoO_6 and the nucleophilic N sites of 2-mbIM, respectively. The regulation of the electron occupancy in the Co ion's eg orbitals induces a transition from the Co^{3+} high-spin state to the moderately spin-polarized Co^{4+} state. The low-energy Co^{4+} orbitals effectively accept σ orbital electrons from N_2 and subsequently transfer electrons to its empty π^* orbitals (Fig. 9b). When N_2 binds to the adjacent CoO_6 octahedron, the Gibbs free energy for the CO_2 reduction reaction decreases from 0.60 eV to 0.52 eV (Fig. 9c), indicating that the presence of N_2 facilitates CO_2 reduction and initiates the C–N coupling reaction to form the NCON urea precursor structure, lowering the reaction barrier to 0.36 eV (Fig. 9d) and ultimately enabling efficient urea synthesis.

MOF catalysts have demonstrated remarkable potential in the field of ESU. However, research on single-atom-based MOF catalysts within this field remains in its nascent exploratory stage, with a paucity of reports available in the extant literature. This research gap poses both a scientific challenge and a significant opportunity for scientific advancement and practical applications.

3.4 Metal oxides

Metal oxides, when utilized as supports for SACs, assume a pivotal role in the electrocatalytic urea synthesis process. This

is primarily attributable to their abundant oxygen coordination environments and exceptional chemical stability. Metal single atoms generally attain stable atomic dispersion by forming robust M–O coordination bonds with oxygen atoms on the support surface. This coordination structure plays a pivotal role in the prevention of aggregation of single atoms. Additionally, it exerts a substantial influence on the adsorption modes and activation energy barriers of reactants by means of electronic structure tuning at the metal center. This, in turn, leads to enhanced catalytic activity and selectivity. The coordination environment for SACs is influenced by the unique crystal structures and surface chemical properties of the metal oxide supports, which can result in multiple reaction pathways. Furthermore, oxygen vacancies and defect structures in the supports themselves play pivotal roles in modulating the electronic properties of the catalysts and stabilizing reaction intermediates, becoming significant design parameters to enhance electrocatalytic urea synthesis performance.

In order to enhance the performance of metal oxide-supported SACs in electrocatalytic urea synthesis (UECN), various design strategies have been adopted, with support selection and defect engineering regarded as critical factors. For instance, Zhang *et al.*[56] anchored zinc single atoms on an oxygen-vacancy-rich In_2O_{3-x} support, finding that the In/Zn_1 sites and oxygen vacancies synergistically promote urea synthesis through a tandem catalytic mechanism. Specifically, the Zn sites activate NO_3^-, while the In sites catalyze CO_2 reduction; their cooperative effect accelerates urea formation (Fig. 10a). This study underscores the significance of the synergy between oxygen vacancies and SACs in the fabrication of high-performance UECN catalysts. It also enhances the comprehension of the tandem catalytic mechanism for NO_3^-/CO_2 reduction to urea. Building on this, Zhang *et al.*[57] further designed an atomically dispersed Cu catalyst supported on In_2O_3 (Cu_1/In_2O_3). The Cu sites catalyze the reduction of NO_3 to NH_2, while the intermediate CO generated at the In sites migrate to the Cu sites, where the C–N coupling reaction occurs (Fig. 10b). The computational results indicate that the transition state energy barrier in the Cu_1–In_2O_3 system is considerably lower than that of pure In_2O_3. This finding suggests that the formation of the $*CONH_2$ intermediate at the Cu_1–O_2–In sites is more favorable (Fig. 10c). This phenomenon is primarily attributed to the relay catalytic synergy between Cu_1–O_2–In and In sites, which effectively promotes the kinetics of urea synthesis. The formation of $*CONH_2$ is followed by an exothermic urea generation process, and thus the catalyst exhibits an excellent urea production rate of 28.97 mmol h^{-1} g^{-1} and a FE of 50.88% in a flow cell.

Conversely, Cao *et al.*[58] developed a low-valence Cu-doped anatase TiO_2 nanotube catalyst that is abundant in oxygen vacancies. Cu doping facilitates the formation of abundant oxygen vacancies and dual Ti^{3+} defect sites in TiO_2, enabling NO_2^- to adsorb laterally on bi-Ti^{3+} active sites. Subsequently, NO_2^- undergoes multi-proton-coupled electron transfer to break the N–O bond, significantly enhancing its adsorption and activation capabilities (Fig. 10d). X-ray photoelectron spectroscopy (XPS) of the catalyst further confirms the presence of oxygen vacancies and Ti^{3+} defects: the O 1s spectra show a pronounced oxygen vacancy signal, and the Ti 2p spectra reveal increased intensity of low-valence Ti^{3+} peaks, indicating that Cu doping effectively induces defect formation (Fig. 10e and f). These defect sites offer advantageous adsorption and activation sites for reactants, thereby markedly enhancing catalytic performance. At a low overpotential of −0.4 V, this catalyst achieves a urea production rate of 20.8 μmol h^{-1} and a FE of 43.1%.

Sun *et al.*[59] designed a novel nickel-confined indium oxide ($Ni–In_2O_3$) electrocatalyst capable of electrochemical co-reduction of nitrate and CO_2 to urea under ambient conditions. In this catalyst, Ni is atomically dispersed, and calculations show that its unique Ni-oxygen vacancy local structure effectively modulates the electronic configuration of neighboring In and Ni atoms, significantly lowering the energy barrier of the rate-limiting step in the urea synthesis reaction. The catalyst exhibits a high FE of up to 19.6% in the UER. Furthermore, Wei *et al.*[60] reported 18 types of metal single atoms loaded on CeO_2 supports as SACs for electrocatalytic urea synthesis. As demonstrated in Fig. 11a, Cu_1–CeO_2 exhibits a remarkably elevated urea production in comparison to alternative M_1–CeO_2 catalysts, attaining an average of 52.84 mmol h^{-1} g_{cat}^{-1}. Subsequent studies have demonstrated that during electrolysis, Cu single atoms undergo electrochemical reconstruction to form Cu_4 clusters. These clusters subsequently serve as the primary active sites for C–N coupling. As illustrated in Fig. 11b, a dynamic and reversible transformation occurs between Cu_4 clusters and Cu_1 single-atom configurations when the potential switches from working potential to open circuit potential. This dynamic structural rearrangement is critical for ensuring the structural stability of the catalyst and its electrochemical performance.

In addition to catalyst design strategies, the influence of cations on electrocatalytic systems has also emerged as a significant research area. Tu *et al.*[61] found that alkali metal cations, particularly K^+, play a crucial role at the electrode/electrolyte interface. They promoted the assembly of reaction intermediates and reduced the activation energy barrier for C–N bond formation. This results in a record urea production rate of 212.8 mmol h^{-1} g^{-1}. Fig. 11c illustrates that, during the synergistic proton–electron transfer process, the ONCONO intermediate sequentially reduces to key species, such as ONCON and *NCON. Ultimately, these species produce urea after four proton–electron transfer steps. Fig. 11d shows that K^+ modulates the electronic structure and spatial configuration of intermediates. This effectively reduces the energy barriers for adsorbate transformations during the reaction. Thus, it facilitates the overall electrocatalytic urea synthesis process and greatly enhances catalytic efficiency. This cation-regulated intermediate assembly strategy not only reveals the multiple regulatory mechanisms of alkali metal ions in electrocatalytic reactions but also demonstrates their broad application prospects in the electrocatalytic synthesis of nitrogen-containing amines and amides.

Despite significant progress, there are still many challenges with metal oxide-supported SACs in electrocatalytic urea synthesis, including further improving urea faradaic efficiency and yield of urea, enhancing the long-term stability of the catalyst, deepening mechanistic understanding, and developing more

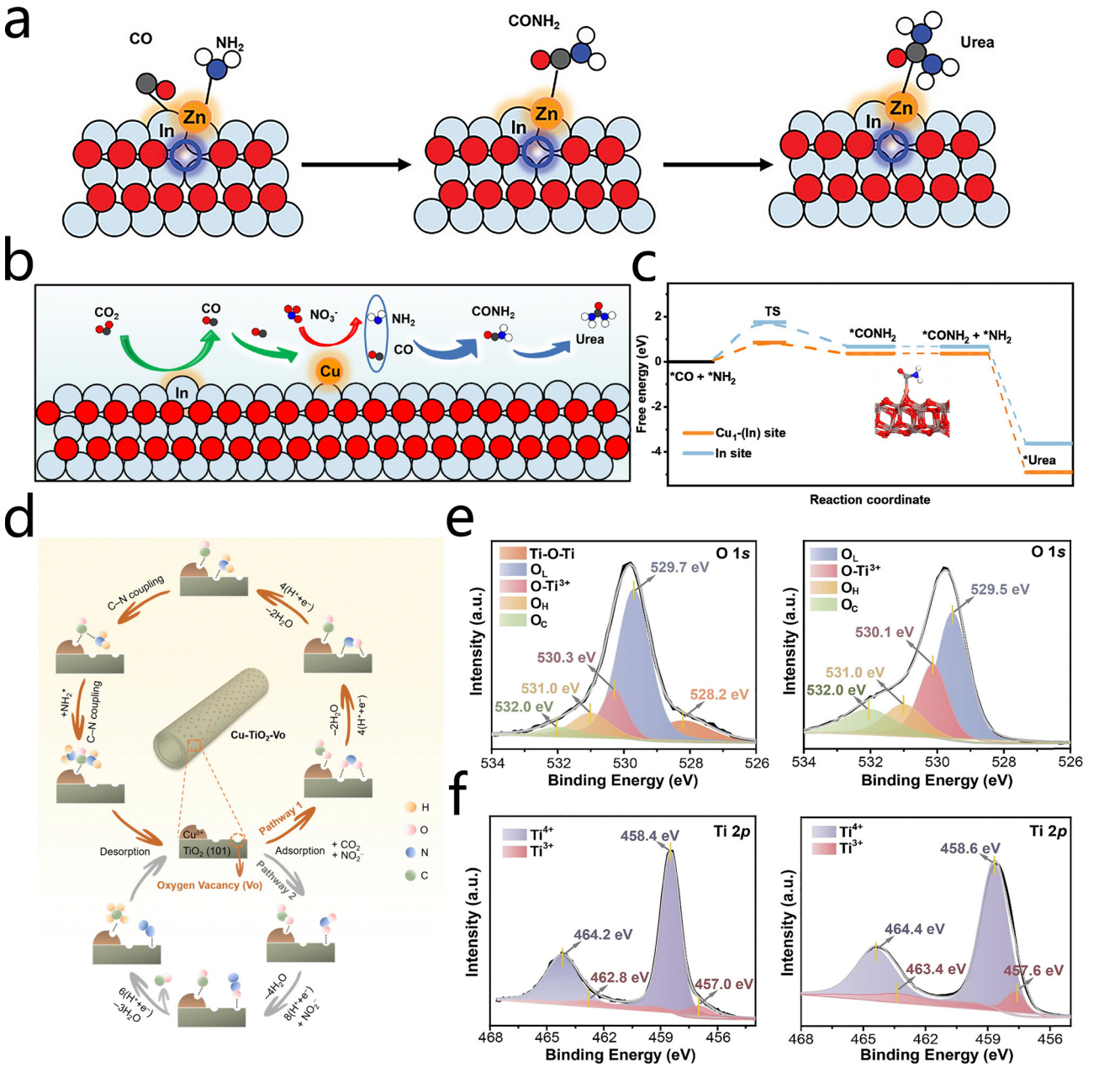

Fig. 10 (a) Schematic for the tandem UECN catalytic mechanism of Zn_1/In_2O_{3-x}. Reproduced with permission from ref. 56. Copyright 2024, Advanced Energy Materials. (b) Schematic for the relay UENC catalytic mechanism of Cu_1/In_2O_3. (c) Free energy diagrams for the electrocatalytic C–N coupling of *CO and $*NH_2$ on In_2O_3 and Cu_1/In_2O_3. Reproduced with permission from ref. 57. Copyright 2024, ACS Nano. (d) Schematic diagram of $CuWO_4$ bimetallic alloys for highly efficient catalytic nitrate synthesis of urea. (e) O 1s XPS spectra comparing undoped TiO_2 and Cu-doped TiO_2. (f) Ti 2p XPS spectra comparing undoped TiO_2 and Cu-doped TiO_2. Reproduced with permission from ref. 58. Copyright 2020, Journal of Colloid and Interface Science.

advanced *in situ* characterization techniques.[62–64] Future research should address these issues, explore innovative catalyst design strategies, optimize reaction conditions, and advance high-resolution *in situ* characterization methods to accelerate the practical application of electrocatalytic urea synthesis technology.

3.5 Recent advances and performance comparison of single-atom catalysts

To systematically present the catalytic performance of representative SACs for electrochemical urea synthesis, Table 1 summarizes key parameters including applied potential *versus* RHE, faradaic efficiency (FE), urea yield rate, and corresponding references. This comparative overview facilitates a clear understanding of the advantages and limitations of different SAC systems, highlighting critical factors influencing catalytic activity and selectivity.

As shown in Table 1, the optimal working potentials, faradaic efficiencies, and urea production rates exhibit substantial variation among the various catalysts. Notably, W and Cu single-atom catalysts supported on MoS_2 exhibit relatively

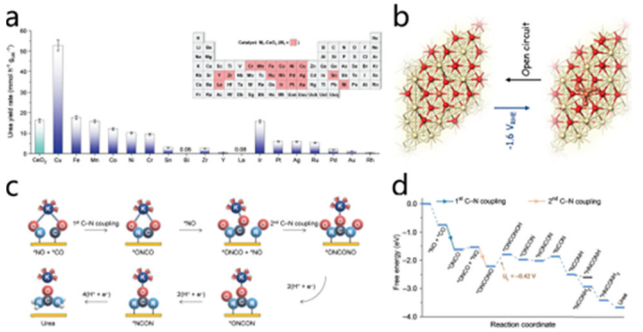

Fig. 11 (a) Stability test results of L-Cu_1–CeO_2 and CuO–CeO_2 catalysts. (b) Schematic diagram of reconstitution of copper single-atoms to clusters suggested by the *operando* XAS measurements. Reproduced with permission from ref. 60. Copyright 2023, Advanced Materials. (c) Schematic diagram of K^+-mediated urea synthesis. (d) Free energy diagram of urea synthesis on single-atom Co decorated TiO_2(101) with the cation effect considered. Reproduced with permission from ref. 61. Copyright 2024, Angewandte Chemie International Edition.

Table 1 Comprehensive performance comparison of SACs for electrocatalytic urea synthesis

Catalysts	V *vs.* RHE	FE (%)	mmol $(g \times h)^{-1}$	Ref.
Cu–GS-800	−0.9	28	30.67	45
N–C-1000	−1.5	2.17	10.18	46
Cu–MoS_2	−0.6	57.02	23.3	50
Fe–MoS_2	−0.5	54.98	18.98	51
W–MoS_2	−0.6	60.11	35.80	52
Co-PMDA-2-mbIM	−0.5	48.97	14.47	55
Zn–In_2O_3	−0.7	55.8	41.6	56
Cu–In_2O_3	−0.6	50.88	28.97	57
Ni–In_2O_3	−0.7	19.6%	0.0111	59
Cu–CeO_2	−1.6	5.29	52.84	60
Co–TiO_2	−0.8	36.2	212.8	61

high FE and yield, thereby demonstrating the advantages of two-dimensional materials in tuning active sites. The Co–TiO_2 catalyst exhibits an exceptional urea yield rate, underscoring the pivotal function of the support in modulating catalytic performance. Future research endeavors should prioritize the optimization of synergistic interactions between metal centers and supports, with the objective of further enhancing catalytic efficiency and stability.

4 Conclusions and outlook

In recent years, catalysts based on SACs have gradually become a popular research topic in the field of catalysis due to their unique structural characteristics and excellent physicochemical properties. The development of precise synthesis strategies and systematic pre-design methods is urgently needed in this emerging field to efficiently regulate the catalyst structure and performance. This study provides a comprehensive review of the research progress of SACs based on carbon-based materials, two-dimensional materials, metal–organic frameworks, and metal oxide supports. The study also provides an in-depth analysis of the regulatory mechanisms by which supports influence the electronic structure and coordination environment of active centres. Particular emphasis is placed on the key reaction mechanisms of C–N bond formation under different nitrogen sources (N_2, NO, NO_2^-, and NO_3^-). While challenges remain in this field, such as synthesis complexity, active site stability, and unclear reaction mechanisms, synergistic innovation between theory and experiment is expected to advance the design and optimization of highly efficient electrocatalytic urea synthesis catalysts, thereby contributing to the development of sustainable energy and green chemistry.

4.1 Prospects

Deep integration of theoretical calculations and experimental studies. Future efforts should focus on strengthening the integration of theoretical calculations and experimental research in order to develop more accurate catalytic models. Combining DFT calculations with *ab initio* molecular dynamics simulations allows us to systematically screen potential highly efficient catalysts and predict reaction pathways and energy barriers.[65,66] Volcano plots constructed based on descriptors such as the d-band center position and charge density transfer, for example, facilitate an understanding of the intrinsic relationship between catalytic activity and electronic properties. However, computational results must be rigorously validated by precise experiments to create a virtuous cycle where theory guides experiments and experiments verify theory. This accelerates the process of designing and optimizing catalysts.

Synergistic catalysis strategy with multiple active sites. Future research should focus on designing SACs with multiple types of active sites in order to achieve the synergistic activation of CO_2 and nitrogen sources.[67] For instance, Ru–Cu bimetallic single-atom alloy catalysts demonstrate synergistic effects, with Ru and Cu sites promoting the activation of NO_3^- and CO_2, respectively, which significantly enhances urea synthesis efficiency. Similarly, constructing dual active sites or relay catalytic systems on metal oxide supports, such as the cooperative effect between Cu_1–O_2–In sites and In sites in Cu_1/In_2O_3 catalysts, represents an effective strategy. Rationally designing multi-active-site structures and optimizing electronic transfer and spatial configuration among active components are expected to result in more efficient C–N coupling reactions.

Sustainable preparation processes and system integration. Developing green and sustainable preparation methods for SACs is a crucial area of future research. Many current synthetic approaches use toxic precursors or involve high-energy processes that are incompatible with sustainability goals. Exploring biotemplate methods, green solvent-assisted synthesis, and low-temperature preparation techniques holds promise for reducing the environmental impact of catalyst fabrication.[68,69] Furthermore, integrating electrocatalytic urea synthesis technology with renewable energy systems, such as solar and wind power, is essential for establishing a complete, carbon-neutral urea production process for industrial application. This includes optimizing electrolyzer design, system integration, and conducting a comprehensive life cycle assessment.

4.2 Challenges

Despite the considerable promise inherent in the development and application of SACs in the field of energy conversion, significant challenges persist with regard to cost and performance. Despite advancements in novel synthesis approaches, such as doping with transition metal atoms and compositional tuning to enhance stability and activity, several critical issues remain unresolved.

Enhancement of catalytic activity and selectivity. Despite the noteworthy advancements in the field of SACs for electrocatalytic urea synthesis, a consensus on a unified standard for industrial application remains elusive. It is widely acknowledged that achieving a stable faradaic efficiency that exceeds 60%, in conjunction with high production rates and long-term stability, is imperative to meet the economic and efficiency demands of industrial production. The highest reported faradaic efficiency to date is approximately 60.11%, which falls short of the threshold for industrial use. The main challenges lie in enhancing the selectivity of the C–N bond coupling reaction while suppressing competitive side reactions such as the hydrogen evolution reaction and isolated CO_2 reduction. Particularly when N_2 is used as a nitrogen source, the high stability of the $N{\equiv}N$ triple bond limits activation efficiency, thereby constraining urea synthesis performance. Moreover, the choice of nitrogen source (*e.g.*, N_2, NO, NO_2^-, and NO_3^-) significantly affects catalytic performance, and further optimization of nitrogen sources under different reaction systems remains necessary.[70]

Catalyst structural stability issues. Despite the demonstrated efficacy and selectivity of SACs in catalytic reactions, their practical applications remain constrained by challenges related to structural stability and large-scale synthesis. Under electrocatalytic reaction conditions, single atoms exhibit a propensity for migration, aggregation, or leaching, particularly when the interaction between the metal atom and the support is inadequate. This phenomenon results in a deterioration in catalytic performance over time. Furthermore, the electronic structure of SACs may result in excessively strong binding with reactants, products, or intermediates, which can lead to poisoning or loss of the active sites and further affect the catalyst's lifetime and efficiency. It has been demonstrated in previous studies that, for instance, copper-based SACs can reorganize into metal clusters during electrolysis. While these kinds of dynamic structural alterations can, on occasion, augment activity, they concomitantly introduce greater complexity to the elucidation of reaction mechanisms. Concurrently, contemporary synthetic methodologies for SACs are predominantly intricate, expensive, and yield-constrained, impeding the capacity to satisfy the requirements of substantial-scale, eco-friendly, and cost-effective industrial production. The mechanisms by which different support materials (*e.g.*, carbon-based materials, two-dimensional materials, MOFs, metal oxides, *etc.*) affect the stability of single atoms have not yet been fully elucidated, which poses further challenges for the design of long-term stable and efficient single-atom catalytic systems. Consequently, the development of robust supports, the enhancement of metal–support interactions, and the exploration of innovative scalable synthesis strategies are imperative for the promotion of the practical application of SACs.

Reaction mechanism and kinetic studies. Despite the recent advancements in elucidating the reaction mechanisms of electrocatalytic urea synthesis (ESU), numerous aspects of the process remain unclear, controversial, or opaque. There is a need for further investigation into the detailed mechanisms of the key steps of ammonia oxidation, CO_2 reduction, and nitrogen heterocycle formation. Additionally, precise control over the kinetics and reaction rates of ESU continues to represent a formidable challenge. It is imperative to prioritize the advancement of knowledge concerning the kinetic characteristics and reaction mechanisms of ESU in the coming years. The identification of rate-determining steps and the elucidation of intricate electrocatalytic reaction pathways are instrumental in optimizing reaction conditions and catalyst system design, thus enhancing the efficiency and selectivity of urea synthesis.

Differences and contradictions in literature data. It is noteworthy that for similar catalysts, there are significant discrepancies in the reported faradaic efficiencies and urea yields across different studies. These discrepancies primarily stem from variations in experimental setups, electrolyte compositions, catalyst loading methods, and differences in product quantification techniques. For instance, certain studies have documented abnormally high faradaic efficiencies, which prove to be challenging to replicate. This has led to apprehensions regarding the reliability of the data and the potential for false-positive outcomes due to contamination or misidentification of products. Therefore, the establishment of standardized testing protocols and the promotion of interlaboratory data cross-validation are essential for accurately assessing and comparing the true catalytic performance of SACs. The establishment of a robust experimental reporting framework is imperative for ensuring the optimal development of this field.

Challenges in urea quantification and byproduct differentiation. In the study of electrocatalytic urea synthesis, accurate quantification of urea and differentiation of byproducts (such as ammonia) remain major challenges. A multitude of prevalent detection methodologies (such as colorimetric and enzymatic assays) are vulnerable to interference from ammonia, nitrate, or other nitrogen-containing species, resulting in an overestimation of urea yields. Furthermore, environmental contamination or incomplete removal of precursors can also result in false-positive outcomes. To address these challenges, it is advisable to utilize isotope labeling techniques in conjunction with advanced analytical methods such as nuclear magnetic resonance (NMR) and mass spectrometry, to ensure the accuracy of product identification and quantification. Cross-validation employing a variety of methods and meticulous control experiments is imperative for ensuring the precision and reproducibility of results.

Challenges in industrial scale-up. The industrial application of electrocatalytic urea synthesis technology is confronted with numerous challenges, including the large-scale production of catalysts, cost control, the design of electrolyzers, and system integration. Currently, a majority of research studies remain at the stage of performance evaluation in small-scale electrolyzers,

lacking comprehensive validation of catalyst long-term stability and system reliability under practical industrial conditions. The feasibility of this technology is assessed by several key metrics, including energy efficiency, carbon footprint, and economic comparison with the conventional Haber–Bosch process. In order to promote commercialization, it is necessary to optimize the electrolyzer architecture, enhance the current efficiency and product yield, and ensure efficient catalyst loading. Integration of this technology with renewable energy sources and waste gas recycling processes can result in an environmentally friendly and sustainable urea production system. Furthermore, economic viability and sustainability are fundamental factors in ensuring market competitiveness and must be meticulously considered in both design and application.

Author contributions

Zhiwei Wang: writing – original draft. Mingying Chen and Guolong Lu: data curation. Jianben Xu and Longchao Zhuo: review and editing. Yinghong Wu and Xijun Liu: supervision, resources, and conceptualization.

Conflicts of interest

There are no conflicts to declare.

Data availability

No primary research results, software or code have been included, and no new data were generated or analysed as part of this review.

Acknowledgements

This work was financially supported by the Guangxi Natural Science Fund for Distinguished Young Scholars (2024GXNSFFA010008), the National Natural Science Foundation of China (22469002), and Pioneer "Hundred Talents Program" of CAS.

Notes and references

1 Z. Liu, Z. Li, S. Chen and W. Zhou, *J. Hazard. Mater.*, 2023, **453**, 131404.
2 W. Shi, Y. Ju, R. Bian, L. Li, S. Joseph, D. R. G. Mitchell, P. Munroe, S. Taherymoosavi and G. Pan, *Sci. Total Environ.*, 2020, **701**, 134424.
3 Zahoor, W. Wang, X. Tan, Y. Guo, B. Zhang, X. Chen, Q. Yu, X. Zhuang and Z. Yuan, *J. Cleaner Prod.*, 2021, **284**, 125392.
4 Y. Ren, C. Yu, X. Tan, H. Huang, Q. Wei and J. Qiu, *Energy Environ. Sci.*, 2021, **14**, 1176–1193.
5 S. Zhang, M. Jin, H. Xu, X. Zhang, T. Shi, Y. Ye, Y. Lin, L. Zheng, G. Wang, Y. Zhang, H. Yin, H. Zhang and H. Zhao, *Energy Environ. Sci.*, 2024, **17**, 1950–1960.
6 L. Y. Stein, *Environ. Microbiol.*, 2023, **25**, 102–104.
7 G. Qing, R. Ghazfar, S. T. Jackowski, F. Habibzadeh, M. M. Ashtiani, C.-P. Chen, M. R. Smith, III and T. W. Hamann, *Chem. Rev.*, 2020, **120**, 5437–5516.
8 B. H. R. Suryanto, H.-L. Du, D. Wang, J. Chen, A. N. Simonov and D. R. MacFarlane, Nature, *Catalysis*, 2019, **2**, 290–296.
9 Y. Wan, J. Xu and R. Lv, *Mater. Today*, 2019, **27**, 69–90.
10 J. H. Montoya, C. Tsai, A. Vojvodic and J. K. Nørskov, *ChemSusChem*, 2015, **8**, 2180–2186.
11 X. Zhu, X. Zhou, Y. Jing and Y. Li, *Nat. Commun.*, 2021, **12**, 4080.
12 J. H. Baik, S. D. Yim, I.-S. Nam, Y. S. Mok, J.-H. Lee, B. K. Cho and S. H. Oh, *Top. Catal.*, 2004, **30**, 37–41.
13 M. Jiang, M. Zhu, M. Wang, Y. He, X. Luo, C. Wu, L. Zhang and Z. Jin, *ACS Nano*, 2023, **17**, 3209–3224.
14 X. Cui, C. Tang and Q. Zhang, *Adv. Energy Mater.*, 2018, **8**, 1800369.
15 Y. Li, Z. He, F. Wu, S. Wang, Y. Cheng and S. Jiang, *Mater. Rep.: Energy*, 2023, **3**, 100197.
16 J. Yang, W.-H. Li, K. Xu, S. Tan, D. Wang and Y. Li, *Angew. Chem., Int. Ed.*, 2022, **61**, e202200366.
17 E. Zhang, L. Tao, J. An, J. Zhang, L. Meng, X. Zheng, Y. Wang, N. Li, S. Du, J. Zhang, D. Wang and Y. Li, *Angew. Chem., Int. Ed.*, 2022, **61**, e202117347.
18 T. Wei, J. Zhou and X. An, *Mater. Rep.: Energy*, 2024, **4**, 100285.
19 Y. Ji, Z. Yu, L. Yan and W. Song, *China Powder Sci. Technol.*, 2023, **29**, 100–107.
20 J. Lin, A. Wang, B. Qiao, X. Liu, X. Yang, X. Wang, J. Liang, J. Li, J. Liu and T. Zhang, *J. Am. Chem. Soc.*, 2013, **135**, 15314–15317.
21 B. Han, R. Lang, B. Qiao, A. Wang and T. Zhang, *Chin. J. Catal.*, 2017, **38**, 1498–1507.
22 H. Wei, X. Liu, A. Wang, L. Zhang, B. Qiao, X. Yang, Y. Huang, S. Miao, J. Liu and T. Zhang, *Nat. Commun.*, 2014, **5**, 5634.
23 X. Guo, G. Fang, G. Li, H. Ma, H. Fan, L. Yu, C. Ma, X. Wu, D. Deng, M. Wei, D. Tan, R. Si, S. Zhang, J. Li, L. Sun, Z. Tang, X. Pan and X. Bao, *Science*, 2014, **344**, 616–619.
24 D. A. Bulushev, M. Zacharska, A. S. Lisitsyn, O. Y. Podyacheva, F. S. Hage, Q. M. Ramasse, U. Bangert and L. G. Bulusheva, ACS, *Catalysis*, 2016, **6**, 3442–3451.
25 L. Zhang, Y. Ren, W. Liu, A. Wang and T. Zhang, *Natl. Sci. Rev.*, 2018, **5**, 653–672.
26 S. Liu, T. Wang, L. Elbaz and Q. Li, *Mater. Rep.: Energy*, 2023, **3**, 100178.
27 C. Yang, Z. Li, J. Xu, Y. Jiang and W. Zhu, *Green Chem.*, 2024, **26**, 4908–4933.
28 J. Fu, Y. Yang and J.-S. Hu, ACS, *Mater. Lett.*, 2021, **3**, 1468–1476.
29 A. Vasileff, X. Zhi, C. Xu, L. Ge, Y. Jiao, Y. Zheng and S.-Z. Qiao, ACS, *Catalysis*, 2019, **9**, 9411–9417.
30 Y. Mao, Y. Jiang, H. Liu, Y. Jiang, M. Li, W. Su and R. He, *Chin. Chem. Lett.*, 2024, **35**, 108540.
31 K. Chen, D. Ma, Y. Zhang, F. Wang, X. Yang, X. Wang, H. Zhang, X. Liu, R. Bao and K. Chu, *Adv. Mater.*, 2024, **36**, 2402160.
32 Y. Feng, H. Yang, Y. Zhang, X. Huang, L. Li, T. Cheng and Q. Shao, *Nano Lett.*, 2020, **20**, 8282–8289.
33 H. Zhao, Z. Li, J. Xiang, W. Du and K. Chu, *Chem. Eng. J.*, 2024, **496**, 154256.
34 J. Long, D. Luan, X. Fu, H. Li and J. Xiao, *ACS Catal.*, 2024, **14**, 14678–14687.
35 Y. Huang, R. Yang, C. Wang, N. Meng, Y. Shi, Y. Yu and B. Zhang, *ACS Energy Lett.*, 2022, **7**, 284–291.
36 H. Wan, X. Wang, L. Tan, M. Filippi, P. Strasser, J. Rossmeisl and A. Bagger, *ACS Catal.*, 2023, **13**, 1926–1933.
37 D. Jiao, Y. Dong, X. Cui, Q. Cai, C. R. Cabrera, J. Zhao and Z. Chen, *J. Mater. Chem. A*, 2023, **11**, 232–240.
38 Y. Cao, Y. Meng, R. An, X. Zou, H. Huang, W. Zhong, Z. Shen, Q. Xia, X. Li and Y. Wang, *J. Colloid Interface Sci.*, 2023, **641**, 990–999.
39 L. Kong, D. Jiao, Z. Wang, Y. Liu, Y. Shang, L. Yin, Q. Cai and J. Zhao, *Chem. Eng. J.*, 2023, **451**, 138885.
40 Y. Cheng, J. Chen, C. Yang, H. Wang, B. Johannessen, L. Thomsen, M. Saunders, J. Xiao, S. Yang and S. P. Jiang, *Energy Environ. Mater.*, 2023, **6**, e12278.
41 H. X. Liu, M. Chen, J. Ma, J. Liang, C. Li, C. Chen and H. He, *China Powder Sci. Technol.*, 2024, **30**, 35–45.
42 X. Hu, D. Zhou, H. Wang, W. Zhang, H. Zhong and Y. Chen, *Chin. Chem. Lett.*, 2023, **34**, 108050.
43 L. Cheng, Z. Cheng, M. Fan, Y. Ren, Y. Liu, T. Yuan and Z. Shen, *Electrochim. Acta*, 2023, **470**, 143283.
44 Z.-H. Zhao, R. Jiang, H. Niu, M. Wang, J. Wang, Y. Du, Y. Tian, M. Yuan, G. Zhang and Z. Lu, *J. Colloid Interface Sci.*, 2025, **682**, 222–231.
45 J. Leverett, T. Tran-Phu, J. A. Yuwono, P. Kumar, C. Kim, Q. Zhai, C. Han, J. Qu, J. Cairney, A. N. Simonov, R. K. Hocking, L. Dai, R. Daiyan and R. Amal, *Adv. Energy Mater.*, 2022, **12**, 2201500.
46 C. Chen, S. Li, X. Zhu, S. Bo, K. Cheng, N. He, M. Qiu, C. Xie, D. Song, Y. Liu, W. Chen, Y. Li, Q. Liu, C. Li and S. Wang, *Carbon Energy*, 2023, **5**, e345.
47 Z. Xiong, Y. Xiao and C. Shen, *Chem. Mater.*, 2022, **34**, 9402–9413.

48 Y. Yang, J. Peng, Z. Shi, P. Zhang, A. Arramel and N. Li, *J. Mater. Chem. A*, 2023, **11**, 6428–6439.
49 J. Peng, X. Wang, Z. Wang, B. Liu, P. Zhang, X. Li and N. Li, *Chin. J. Struct. Chem.*, 2022, **41**, 2209094–2209104.
50 W. Du, Z. Sun, K. Chen, Y. Wei, R. Bao and K. Chu, Adv. Energy Mater., *Adv. Energy Mater.*, 2024, **14**, 2401765.
51 W. Du, Z. Sun, S. Shang, K. Chen, X. Yang and K. Chu, *ACS Nano*, 2024, **18**, 27718–27726.
52 D. Yuan, Y. Jiang, W. Du, D. Ma and K. Chu, *J. Colloid Interface Sci.*, 2025, **680**, 36–42.
53 Y. Wan, Z. Zhang, J. Qian, Y. Wei, J. Kang and K. Chu, *Nano Lett.*, 2024, **24**, 10928–10935.
54 S. Zhou, H. Li, H. Gao, A. Li, T. Li, S. Cheng, J. Wang, J. Kasemchainan, J. Yi, F. Zhao and W. Qu, *Chin. Chem. Lett.*, 2025, **36**, 110142.
55 M. Yuan, J. Chen, H. Zhang, Q. Li, L. Zhou, C. Yang, R. Liu, Z. Liu, S. Zhang and G. Zhang, *Energy Environ. Sci.*, 2022, **15**, 2084–2095.
56 Y. Zhang, Z. Li, K. Chen, X. Yang, H. Zhang, X. Liu and K. Chu, *Adv. Energy Mater.*, 2024, **14**, 2402309.
57 Y. Zhang, Z. Li, C. Qiang, K. Chen, Y. Guo and K. Chu, *ACS Nano*, 2024, **18**, 25316–25324.
58 N. Cao, Y. Quan, A. Guan, C. Yang, Y. Ji, L. Zhang and G. Zheng, *J. Colloid Interface Sci.*, 2020, **577**, 109–114.
59 H. Sun, S. Lee, R. Tang, L. Wang, C.-J. Yang, W. Liang, S. Zhao, C.-L. Dong, A. Soon and J. Huang, *Adv. Funct. Mater.*, 2025, **35**, 2415859.
60 X. Wei, Y. Liu, X. Zhu, S. Bo, L. Xiao, C. Chen, T. T. T. Nga, Y. He, M. Qiu, C. Xie, D. Wang, Q. Liu, F. Dong, C.-L. Dong, X.-Z. Fu and S. Wang, *Adv. Mater.*, 2023, **35**, 2300020.
61 X. Tu, X. Zhu, S. Bo, X. Zhang, R. Miao, G. Wen, C. Chen, J. Li, Y. Zhou, Q. Liu, D. Chen, H. Shao, D. Yan, Y. Li, J. Jia and S. Wang, *Angew. Chem., Int. Ed.*, 2024, **63**, e202317087.
62 K. Lian, S. Gao, W. Liu, Q. Liu, Y. Feng, J. Luo, G. Hu, K. Chu, D. Wang and X. Liu, *ACS Nano*, 2025, **19**, 20001–20011.
63 Z. Wang, G. Lu, T. Wei, G. Meng, H. Cai, Y. Feng, K. Chu, J. Luo, G. Hu, D. Wang and X. Liu, *Nat. Commun.*, 2025, **16**, 2885.
64 L. Li, I. Hasan, Farwa, R. He, L. Peng, N. Xu, N. K. Niazi, J.-N. Zhang and J. Qiao, *Nano Res. Energy*, 2022, **1**, 9120015.
65 S. Yang, K. Yang, J. Mi, S. Guo, X. An, H. Su and Y. He, *Mater. Rep.: Energy*, 2025, **5**, 100317.
66 H. Zhang and Y. Wu, *China Powder Sci. Technol.*, 2025, **31**, 1–17.
67 M. Yang, J. Ding, Z. Wang, J. Zhang, Z. Peng and X. Liu, *Chin. Chem. Lett.*, 2025, **36**, 110861.
68 J. Luo, J. Zheng, M. Wu, F. Dong, Y. Liu, J. Qiao and Y. Yang, *Mater. Rep.: Energy*, 2025, **5**, 100327.
69 L. Yang, X. Huang, H. Shan, X. Shu, C. Deng, N. Zhou and K. Hu, *China Powder Sci. Technol.*, 2025, **31**, 113–121.
70 Y. Wang, L. Zhang, C. Wang, Z. Wang, Y. Feng and X. Liu, *Chem. Commun.*, 2025, **61**, 4399–4402.